Ocean Sci. Discuss., 11, 1357–1390, 2014
www.ocean-sci-discuss.net/11/1357/2014/
doi:10.5194/osd-11-1357-2014

Ocean Science
Discussions
Open Access

Observing and modeling currents on the continental slope: assimilation of high frequency radar currents and hydrography profiles

A. K. Sperrevik, K. H. Christensen, and J. Röhrs

Norwegian Meteorological Institute, Oslo, Norway

Received: 11 April 2014 – Accepted: 3 May 2014 – Published: 4 June 2014

Correspondence to: A. K. Sperrevik (ann.k.sperrevik@met.no)

Published by Copernicus Publications on behalf of the European Geosciences Union.

Abstract

Assimilation of High Frequency (HF) radar current observations and CTD hydrography is performed with the 4D-Var analysis scheme implemented in the Regional Ocean Modeling System (ROMS). We consider both an idealized case, with a baroclinic slope current in a periodic channel, and a realistic case for the coast of Vesterålen in Northern Norway. In the realistic case the results of the data assimilation are compared with independent data from acoustic profilers and surface drifters. Best results are obtained when background error correlation scales are small (10 km or less) and when the data assimilation window is short, i.e. about one day. Furthermore, we find that the impact of assimilating HF radar currents is generally larger than the impact of CTD hydrography, which implies that the amount of hydrographic data is insufficient to constrain the solution. Combining the HF radar currents with a few hydrographic profiles gives significantly better results, which demonstrates the importance of complementing surface observations with observations of the vertical structure of the ocean.

1 Introduction

Skillful ocean forecasts are of key importance for many operations at sea, especially for emergency response services such as search and rescue and oil spill mitigation. In particular, near-surface currents are an important input to operational drift forecast models. However, the predictability of ocean currents remains a challenge due to their turbulent nature and high spatial variability, for example associated with eddies.

Observations of the ocean surface temperature (Wentz et al., 2000; Rayner et al., 2003) and elevation (Fu et al., 1994) from satellites have become plentiful during the last decades. New satellite observations include surface salinity and currents, but the uncertainty of these products still remains too high for use in models with high horizontal resolution, i.e. at the order of 1 km. Through efforts such as the International Argo Program (Roemmich et al., 2009), observations of the subsurface ocean are increasing

OSD
11, 1357–1390, 2014

in number, but still remain too few to resolve the vertical and horizontal density structure of e.g. oceanic fronts.

Advanced data assimilation (DA) techniques developed in the field of numerical weather prediction are now used to a great extent within ocean modeling. The DA schemes range from multivariate implementations of optimal interpolation, such as Ensemble Optimal Interpolation (Oke et al., 2010) in the Australian Bureau of Meteorology's Bluelink forecast system (Brassington et al., 2007), to ensemble Kalman filters (Evensen, 2003) in the TOPAZ4 system (Sakov et al., 2012) and variational methods (Dimet and Talagrand, 1986; Courtier et al., 1994) used in UK Met Office's FOAM (Blockley et al., 2013). Common for these system is that few, if any, current observations are assimilated, mainly owing to a lack of good observations.

HF radars, which can sample surface currents up to 200 km offshore provide an excellent option for mapping surface currents in coastal areas (e.g. Barrick et al., 1977; Chapman et al., 1997; Gurgel et al., 1999). Real time surface currents from HF radars can be used for monitoring and emergency applications, but also for data assimilation to improve the ocean forecasts. Previous studies (see Breivik and Sætra, 2001; Oke et al., 2002; Paduan and Shulman, 2004; Barth et al., 2008; Zhang et al., 2010, for some examples) demonstrate the potential of HF radar current observations in ocean data assimilation systems.

The aim of this study is to investigate whether assimilation of current observations from a rapid-deployable HF radar system (Kjelaas and Whelan, 2011) in a high resolution ocean model is a feasible way to improve the regional ocean forecast during e.g. an oil spill event. This requires an ocean forecast system which is ready to use such observations as soon as they become available. We have used the incremental, strong-constraint four-dimensional variational data assimilation (IS4DVAR) driver of the Regional Ocean Modeling System (ROMS) described in detail in Moore et al. (2011c, a, b). The model is implemented for a region in Northern Norway, which is characterized by a strong northward slope current and high eddy kinetic energy. The tidal signal in this area is also significant. We show that the skill of the predictions produced by

OSD
11, 1357–1390, 2014

the ocean forecast system indeed increases after just one assimilation cycle when HF radar total currents are included. Including in-situ hydrography profiles to the assimilated observational data set, adds an additional constraint on the circulation.

We start by describing the observational data sets in Sect. 2. In Sect. 3 we present an idealized assimilation experiment, before a realistic experiment is presented and compared with independent observations in Sect. 4. A summary and some concluding remarks are is given in Sect. 5.

2 Field campaign and observation network

An array of three SeaSonde HF radars, manufactured by CODAR Ocean Sensors, were deployed along the coast of Vesterålen in Northern Norway in the first week of March 2013. All three stations were de-mobilized in the beginning of June 2013. The operating frequency of the radars were 13.525 MHz, thus measuring the Bragg backscatter from waves with wavelength of about 11 m. The errors in the HF radar observations are mainly due to geometrical dilution of precision (Chapman et al., 1997), and each observation data file transmitted by the HF radar system contained estimates of the observation errors. Typically these errors were less than 20 % of the observed values within a distance of about 40 km of the radars, gradually increasing to almost 100 % near the limits of their range. To account for discrepancies in observed and modelled tides, HF radar currents are usually subjected to a correction of the tidal signal before assimilation, as described in Zhang et al. (2010). As our time series is too short to provide a good estimate of the observed tidal signal, no such corrections have been made. This would, however, also be the case during a realistic event, and our results are thus a demonstration of the potential impact of a rapid-deployable HF radar system.

The main motivation for deploying the radars in this part of Norway was the co-location with the annual cod stock assessment cruise of the Institute of Marine Research (IMR) (see Fig. 1). Hydrographic and acoustic data are routinely collected during these cruises, and surface drifters were deployed from the research vessel R/V

OSD
11, 1357–1390, 2014

Johan Hjort as it passed the area covered by the HF radars (see Fig. 2). A total of 14 surface drifters from MetOcean, Canada, were used in the field campaign. Seven of these were "iSphere" type drifters, which are spherical surface floats that are half submerged, and the other seven were "iSLDMB" drifters with a drogue centered at 65 cm below the surface. The precision of the reported GPS positions are approximately 10 m, implying an error circle of radius of 10 m. The analysis in Sect. 4.3.1 focus on three hour long trajectory segments, during which the buoys in question travelled an average of ~ 2700 m. The error is thus less than 1 % of the observed distance. Previous studies have shown that the behavior of these types of surface drifters can be markedly different, mainly depending on the wind and wave conditions (Röhrs et al., 2012).

Prior to the cod stock assessment cruise we deployed a rig with three separate acoustic Doppler current profilers (ADCPs). The total water depth at the site was 86 m, its location is shown in Fig. 2. Two Anderaa RDCP 600 kHz were mounted at about 40 m depth, one upward looking and one downward looking, in addition to an upward looking 1 MHz Nortek Aquadopp Profiler at about 10 m depth. The observed ocean currents at 1 m depth from the Nortek Aquadopp ADCP had a variability (standard deviation) of 17 cm s^{-1}. The accuracy is 2 cm s^{-1} for 30 min averaged samples. This accuracy is obtained as the mean error of the 30 min averages, given by the standard deviation of bootstrapped samples in each averaging period.

3 Idealized experiments

Prior to applying the assimilation system to a realistic case we investigate various options associated with the IS4DVAR scheme using an idealized setup. More specifically, the IS4DVAR scheme is tested for an idealized case of strongly nonlinear, unstable baroclinic flow along a steep slope. The impact of varying the horizontal error correlation scales, the number of inner and outer loops, as well as the length of the assimilation window is assessed to provide an indication on how to configure the assimilation system for the realistic case later on. The tests are set up such that the model system is

OSD
11, 1357–1390, 2014

essentially without any systematic error (bias) and the evaluation of the test cases is primarily based on the standard deviation of the analysis error. We use a linear equation of state, and density changes are accommodated by imposing surface and bottom heat fluxes, hence salinity plays no role in the idealized experiments.

There are seven dependent variables in ROMS: $(u, v, T, S, \zeta, \overline{u}, \overline{v})$, representing horizontal velocity in easterly direction, horizontal velocity in northerly direction, potential temperature, salinity, vertically averaged velocity in easterly direction, vertically averaged velocity in northerly direction, and sea surface height, respectively.

3.1 Model grid

The model domain is configured as a channel with periodic north-south boundary conditions and solid walls along the eastern and western boundaries. The grid is Cartesian with a horizontal resolution of 2.4 km. We use the f-plane approximation with constant Coriolis parameter equivalent to 65° north. The domain size is 100 × 120 interior grid points (easterly/northerly directions), and we use 35 vertical levels.

The main topographic features are (i) a shelf along the eastern boundary, with average depth of 200 m, and width of approximately 70 km, (ii) a sharp shelf break with a hyperbolic tangent profile (maximum slope is approximately 0.1), and (iii) a deep ocean floor with average depth of approximately 1800 m towards the western boundary. In order to trigger instabilities, the depth is perturbed with random values between −50 m and +50 m.

3.2 Initialization and forcing of the model

The initial conditions are uniform with $T = 10\,^{\circ}\mathrm{C}$, $S = 35\,\mathrm{psu}$, $\zeta = 0\,\mathrm{m}$ and zero velocities. Constant heat fluxes over a period of 150 days are applied. The aim is to produce unstable baroclinic currents that will be guided by topography. To accommodate this, we apply a net bottom heat flux into the ocean on the shelf, and a net surface heat flux out of the ocean over the deep ocean (Isachsen, 2011). These fluxes are exactly balanced,

OSD
11, 1357–1390, 2014

such that the net heat flux into the ocean is zero. Since the deep ocean is wider than the shelf, the surface fluxes are smaller than the bottom fluxes (approximately 160 $W\,m^{-2}$ and 440 $W\,m^{-2}$, respectively). The momentum and net freshwater fluxes are zero.

The water heated over the shelf bottom is rapidly mixed upwards through the entire water column resulting in a sharp temperature front near the shelf break. Due to geostrophic adjustment, a northward flowing, topographically controlled slope current develops. This current is baroclinically unstable and heat exchange with the deep water region is facilitated by macro turbulence (ocean eddies), see Fig. 3.

The domain is periodic so that the water masses flowing out of the domain at the northern boundary reappear at the southern boundary. As shown in Fig. 3, the mean northward surface velocity has a maximum of about 1 $m\,s^{-1}$ over the slope, which means that a drifting object can potentially be advected through the domain in about three days. The flow is also characterized by baroclinic and barotropic waves and eddies with propagation speeds that are generally different from the mean flow speeds. To investigate how upstream conditions influence the dynamics in this region we performed an adjoint sensitivity study (e.g. Moore et al., 2009; Zhang et al., 2009). Focusing on the advection of water masses, hence investigating the sensitivity of the surface velocity variance to temperature, choosing a short section over the slope in the middle of the domain. Based on our results we conclude that an upper limit of three days for the assimilation experiments is adequate.

3.3 Configuration of the data assimilation system

In our experiments, data assimilation is only considered for interior grid points and no adjustment of the surface/bottom fluxes or boundary conditions are made. The 4DVAR schemes implemented in ROMS also has options for multivariate background error correlations, but since the underlying theories are dubious for high latitudes and eddy resolving models, we do not make use of any such options here. The estimates of background errors are taken from day 120 to 150 of the spinup period, using the standard

OSD
11, 1357–1390, 2014

deviation of each variable in each grid point. The vertical error correlation lengths for all variables is set to 30 m.

3.4 Synthetic observations

Synthetic observations are taken from a separate model simulation that has been forced with time varying momentum and heat fluxes. An example of the difference between the simulation used for synthetic observations and the simulation that forms the basis for the assimilation experiments is shown in Fig. 4. The difference between the simulations is primarily related to small scale features associated with the baroclinically unstable current over the slope. An estimate of realistic observation errors are assigned to the synthetic observations for use in the assimilation system, but no random or systematic errors are added to the observation values themselves.

The observation locations are shown in Fig. 5. Hydrographic observations, e.g. such as taken from a research vessel with a CTD, are simulated by taking a single vertical profile of temperature every hour, zigzagging southwards with four sections across the slope. A total of 64 temperature profiles are processed and each individual observation is assigned a constant error of 0.05 K. Two simulated HF radars are used to provide hourly total current vectors in 61 locations. These HF radar stations are positioned a distance of $y_a = 118$ km and $y_b = 166$ km from the southern boundary.

We assume that the HF radars retrieve radial currents from an effective depth $D_e = 2$ m, with an azimuthal resolution of $\Delta\theta = 11.25^\circ$. Furthermore we assume that the maximum range of the radars is $R = 80$ km, and that the relative observation error σ_R associated with the radial currents is a linear function of radial distance r. The azimuthal resolution determines the number of beam directions, and, combined with the maximum range R, also the number of intersecting beams from which we can estimate total current vectors.

To obtain the synthetic HF radar observation errors we have first used standard vector algebra to determine the positions were the beams intersect and then calculated the errors in the easterly and northerly directions ($\sigma^{(E)}_{GDOP}, \sigma^{(N)}_{GDOP}$) due to geometric

OSD
11, 1357–1390, 2014

dilution of precision (GDOP) (Chapman et al., 1997). The total errors are then assumed given by

$$\left(\sigma_{\text{tot}}^{(\text{E})}, \sigma_{\text{tot}}^{(\text{N})}\right) = \left(\sigma_{\text{GDOP}}^{(\text{E})}\sigma_{\text{R}}u, \sigma_{\text{GDOP}}^{(\text{N})}\sigma_{\text{R}}v\right), \quad (1)$$

where (u,v) are the observed speeds in the easterly and northerly directions, respectively. The errors in a real HF radar system are more complex than those given by Eq. (1), but a comparison with error statistics from a CODAR SeaSonde system deployed near Fedje in Western Norway indicate that the values obtained from Eq. (1) are reasonable (not shown here).

Finally, in order to cover the region with the most energetic currents near the slope, the entire simulated HF radar system is translated approximately 40 km westwards from the eastern boundary, see Fig. 5.

3.5 Results of the idealized experiments

We only consider the velocities (u,v) and the temperature T in the evaluation of the idealized experiments. Furthermore, we only consider a limited region of interest similar to the HF radar coverage area (see Fig. 3), and also restrict the evaluation to the two uppermost vertical levels of the model. We evaluate a three day period, using sequential data assimilation when the assimilation window is shorter than 72 h.

The procedure is as follows: each model simulation results in an analysis, i.e. a solution of ROMS-4DVAR, which is compared with the "truth" as represented by the simulation that provides the synthetic observations. Average bias and standard deviation for each of the variables (u,v,T) are calculated based on all grid points and all output times in the region of interest. Due to the idealized design of the experiments, the (u,v,T) variables have little bias compared to what we would expect from a realistic model. The standard deviation is used when deciding which options yield the best results.

A total of 15 different model simulations with ROMS-4DVAR have been made. In the simulations we have considered (i) the horizontal background error correlation scales,

OSD
11, 1357–1390, 2014

(ii) re-linearization of tangent linear and adjoint models using so-called outer loops (e.g. Moore et al., 2011c), (iii) length of assimilation window, and (iv) the relative impact of HF radar observations compared to hydrographic observations.

The results show that using a small horizontal error correlation scale of 5 km gives best results (see Table 1); a likely explanation is that observation values are erroneously distributed across sharp gradients when larger correlation scales are used. Furthermore, using outer loops is beneficial, with no significant improvement when using more than two re-linearizations. The length of the assimilation window also plays a role: slight improvement is obtained when reducing the window length from 72 to 24 h, but there is essentially no difference when the window length is further reduced to 6 h. The impact of assimilating HF radar currents is generally larger than the impact of assimilating hydrography, but in both cases we obtain improvement for the temperature. Assimilating hydrography profiles only does not improve the currents, while assimilating HF radar currents has a positive impact on both the velocities and the temperature (see Table 2).

4 Realistic experiments

The realistic experiments were carried out with a model application covering the region of the Lofoten archipelago with 2.4 km horizontal resolution (see Fig. 6). As in the idealized application, there is a shelf in the eastern part of the domain, and a sharp shelf break. The area is characterized by strong northward currents and high eddy kinetic energy levels, which makes this a challenging area for ocean predictions.

4.1 Model grid and forcing data

The model domain of the realistic model simulations is a subset of the operational high resolution ocean model at MET Norway (Albretsen et al., 2011; Röhrs et al., 2014) centered around the Lofoten and Vesterålen archipelago. The model has 35 vertical

OSD
11, 1357–1390, 2014

layers with increased resolution near the surface. As ocean data assimilation requires extensive supercomputing resources, the horizontal resolution has been decreased from 800 m to 2.4 km compared to the operational setup.

The lateral boundary conditions are retrieved from the operational setup at 800 m resolution, using three-hourly fields of sea surface elevation, temperature, salinity, and currents. To remove fine scale features from the high resolution fields, that are unresolved in the coarser grid, the fields are averaged over 3×3 grid points before they are interpolated to the coarser grid.

The simulations use open boundary conditions for sea surface elevation and barotropic currents (Chapman, 1985; Flather, 1976). For tracers and baroclinc velocities, boundary conditions as described in Marchesiello et al. (2001) are used. During assimilation, however, clamped boundary conditions with a sponge layer are applied.

As atmospheric forcing we use hourly fields of air temperature and humidity 2 m above ground, 10 m winds, sea level pressure, cloud cover, and precipitation from MET Norway's operational weather forecast at 4 km resolution (Kristiansen et al., 2009).

A spin-up model simulation was initialized at 15 February 2013 from the smoothed high resolution fields from the operational setup, and run through 15 April 2013. The initial conditions for the assimilation simulations were obtained from the spin-up simulation.

4.2 Configuration of the data assimilation system

The same basic configuration of the assimilation system as in the idealized case (see Sect. 3.3) were used for the realistic experiments. Some tuning of key parameters to optimize the performance is however necessary. The results from a series of tests where the horizontal background correlation scales, number of outer and inner loops, and the length of the assimilation window, were used to determine the parameters of the IS4DVAR system. Based on the outcome of these tests, we proceed with horizontal background error correlation scales of 10 km, 10 inner and 2 outer loops and an assimilation window length of 24 h.

OSD
11, 1357–1390, 2014

The results discussed below stem from a single data assimilation cycle. The experiments are started on 18 March 2013 at 00:00 UTC. IS4DVAR is run for 24 h, assimilating observations collected during this period and producing modified initial conditions for 00:00 UTC, 18 March. Next, a 5 day free simulation is run, initiated from this updated ocean state. In the following discussions, the first day of these simulations is termed "analysis", while the remaining four day period is termed "forecast". This is due to the fact that observations taken within the first 24 h was used during assimilation. It should be noted that the atmospheric forcing used in these experiments is of higher quality than what would have been available in a near real-time setting, which affects the predictability of the ocean forecast.

During the free simulations, simulated surface drifters are released in the positions occupied by the real surface drifters from the field campaign. Simulated surface drifters are released every three hours at the position of the real drifters at that time. The depth of the simulated drifters is set to 65 cm below the sea surface for the simulated iSLDMB drifters, and 10 cm for the simulated iSphere drifters.

This procedure has been repeated three times, with different sets of observations to assess the impact the different observation data sets have on the analysis and subsequent forecast. During the first simulation only CTD hydrography profiles were assimilated, in the following results from this simulation will be denoted "CTD", the second time only HF radar total vectors were included, denoted "HF", while the third simulation assimilated both CTD profiles and HF radar currents, denoted "ALL". Additionally, a control simulation, in which no data assimilation was performed, was conducted for the same time period, with numerical floats released in the same manner as in the assimilation simulations, denoted "CTRL".

4.3 Assimilation performance

We evaluate the performance of the data assimilation system using independent observations from the field campaign (Sect. 2), that is, observations that have not been used during the data assimilation, and therefore serve as an independent measure of

OSD
11, 1357–1390, 2014

skill. We validate the results from the analysis period and the forecast period of the simulations separately.

4.3.1 Comparison with surface drifters

Ocean forecast are used for input to trajectory models, which predict the drift of e.g. oil spills or objects in the sea. Thus, the forecast's ability to reproduce the trajectories of the surface drifters is a good measure of forecast skill. The trajectories of the iSLDMB surface drifters released during the field campaign are compared with their numerical twin from the free simulations following the same methods as used in Röhrs et al. (2012). First, the vector correlation between predicted and observed drifter velocities is evaluated using an analysis similar to the method described in Davis (1985). The trajectories are split into 3 h long segments, and the drift velocities for these segments are then calculated. Defining the vector correlation as:

$$r = 1 - \frac{\left\langle (\boldsymbol{v}_i - \boldsymbol{v}_j)^2 \right\rangle}{\left\langle \boldsymbol{v}_i^2 \right\rangle + \left\langle \boldsymbol{v}_j^2 \right\rangle}, \tag{2}$$

the correlation coefficients r of simultaneous pairs of drifter velocities may be calculated. The results are given as a value between 1 and −1, where a value of 1 means perfect correlation in both speed and direction, a value of 0 means no correlation, while a value of −1 means that the drifters are anti-correlated, i.e. having opposite direction but the same speeds.

The resulting vector correlations between the assimilation simulations and the real drifters are shown in Fig. 7. The quality of the CTRL simulation decreases rapidly, and as the simulation enters into the forecast period, modelled and observed drifter velocities are uncorrelated. The CTD simulation follows the CTRL closely. In fact, the correlation coefficient for the CTD simulation is mostly below the CTRL simulation, indicating that the number of CTD profiles are too sparse to pose a constraint on the

OSD
11, 1357–1390, 2014

circulation and therefore have only minor impact on the subsequent model predictions. Assimilation of HF radar currents, on the other hand, significantly improves the simulated drifter velocities during both the analysis and the forecast period. Note that adding CTD hydrography to the HF currents further improves the model predictions during the first forecast day, which is in contrast to the deterimental effect of only using CTD observations. A likely explanation is that the addition of hydrographic observations acts as an additional constraint of the vertical density structure. This shows how important it can be to constrain all state variables in order to achieve the best possible model predictions.

The significance of the improvement has been tested comparing ALL and CTRL using a Wilcoxon rank-sum test. The improvement in current direction is statistically significant, while not so for the speeds. Our interpretation is that the major benefit of assimilating HF radar currents in these simulations is the correction of the current direction, e.g. adjustments in the positions of eddies and the coastal current. This test does not imply that no improvement in speed is obtained (Fig. 7 indicates that the results are better), but that the impact cannot be statistically verified with the limited observational data available.

The impact of data assimilation is also evaluated by comparing observed and predicted trajectories. For this comparison we use the method presented in Liu and Weisberg (2011), in which not only the end points of the observed and modelled trajectories are compared, but also the entire history of the drifter trajectories. The normalized cumulative Lagrangian separation is defined as:

$$s = \sum_{i=1}^{N} d_i \Big/ \sum_{i=1}^{N} l_{oi}, \tag{3}$$

where d_i is the separation distance between observed and modeled trajectory endpoints at time t_i after initialization, l_{oi} is the length of the observed trajectory and N is

OSD
11, 1357–1390, 2014

the total number of time steps evaluated. A skill score S is then defined as

$$S = \begin{cases} 1 - s, & \text{if } s \leq 1, \\ 0, & \text{if } s > 1. \end{cases} \quad (4)$$

High skill score means that observed and modelled trajectories agree well throughout the period under evaluation.

The skill score is calculated both for the analysis period and for the first 48 h of the forecast period. Results are shown in Table 3 for both types of surface drifters. Assimilation does improve predictions of drifter trajectories, although the impact is more limited compared to the drifter velocities. The results show that the skill improves when we consider periods longer than a day. In these cases, data assimilation seems to constrain the ocean circulation in such a way that the predicted trajectories does not stray as far away from the observed paths as they do in a free simulation, which is probably related to the too low energy levels of the control simulation, as discussed below. Two examples of modelled vs. observed trajectories are shown in Fig. 8.

4.3.2 Comparison with ADCP measurements

We also compare the results from the different model simulations with the speed and direction measured by the ADCPs. The upper ADCP measured currents starting 0.5 m below the surface and down to 8 m in vertical bins of 25 cm, while the lower ADCP measures currents from 41 m to the surface in 1 m bins. From the lower ADCPs, only data below 8 m are used for validation. To evaluate the depth-integrated flow, we integrate from 0.5 m below the surface and down to 8 m for the upper ADCP, while for the lower ADCP we integrate from 8 m and down to 41 m. Transport magnitude and direction, given by the vertically integrated ADCP currents, are compared with the the same quantities calculated from model results.

From inspection of time series of transport magnitude and direction (not shown), we find that the upper ADCP measures a transport with mostly north-northeasterly heading during the period. The CTRL simulation predicts a north-northwest headed current

OSD
11, 1357–1390, 2014

during the period in question. In addition to the discrepancy in direction, the transport magnitude predicted by the CTRL is too weak during the whole simulation in both upper and lower sections. Figures 9 and 10 shows RMS and bias of the different simulations. The figure clearly show that assimilation of hydrography profiles does not enhance the predictions. On the contrary, after the first forecast day the directional RMS error and bias is worse than for the control simulation in both the surface layer and below. Assimilation of HF radar currents, however, has a remarkable effect on both speed and direction, and the predicted current remains more energetic throughout the forecast period. The effect of the assimilation on current direction is also maintained for several days into the forecast. The combination of HF radar currents and CTD further improves the predicted current speed throughout most of the period. Due to a displacement of an eddy in ALL, this simulation performs poorer for the ADCP location than HF and CTRL during the last days of the forecast.

5 Discussion and concluding remarks

In the presented experiments we have assimilated HF radar and hydrography profiles from a time period of only 24 h. Hydrography profiles were sparse in comparison with the number of HF radar current observations. The experiments were carried out for a specific time period and the results are therefore influenced by local weather conditions and do not necessarily represent the variations in predictability of different flow regimes.

HF radar surface currents provide unique information of near-coastal circulation, and as the observations are available in real time it holds the potential to significantly improve ocean forecasts. In this work we have examined the impact of various observations on slope currents in a high resolution ocean data assimilation system.

Starting with an idealized test case with synthetic HF total currents and hydrography profiles being assimilated, we find that it is necessary too keep the horizontal error correlation scales small. The turbulent nature of strong slope currents leads to

OSD
11, 1357–1390, 2014

sharp gradients, and when large correlation scales are used the information provided by the observations may be erroneously spread across fronts. As incremental strong constraint 4DVAR is based on repeated iterations of a tangent linear version of the model and the associated adjoint model, the linearization assumption needs to hold throughout the assimilation window. As slope currents are strongly nonlinear, this window needs to be quite short. Both the idealized and the realistic experiments give best results when the window is 24 h long. We also find that re-linearizing the preliminary solution through a so called outer loop is beneficial for the subsequent model performance. These findings are confirmed when similar experiments are performed with a realistic model with real observational data.

Hydrography observations alone have no positive impact on the surface currents, not even in the idealistic experiments where a quite large number of profiles were assimilated. In the realistic experiments there is even evidence of a deteriorating effect. Constraining the flow regime would require a spatial and temporal density of hydrography profiles over a much longer time period than used in this study. With assimilation of HF currents on the other hand, the current forecasts do improve. Gridded fields of surface currents, with temporal resolution of an hour provide the data assimilation system with improved positioning of eddies and more realistic current speed. In the idealistic experiments we even see improvement in the temperature fields. There are indications that this also holds in the realistic experiments, but independent observations are too sparse to confirm this. Using both HF currents and CTD profiles for assimilation yields thee best results. Although CTD profiles did not improve the current forecasts alone, together with the HF radar surface currents they seem to add an additional constraint on the circulation. These results demonstrate the importance of sampling not only the surface, but also the subsurface density structure.

All results discussed in this work are obtained after performing only one assimilation cycle. We conclude that using HF radars currents in operational data assimilation systems hold the best potential for improving coastal forecasts. Current predictions

OSD
11, 1357–1390, 2014

are significantly improved after only one assimilation cycle, demonstrating the potential benefit of deploying HF radars during e.g. oil spill events.

Acknowledgements. This work was funded by the Norwegian Clean Seas Association for Operating Companies (NOFO) and ENI Norge A/S, with contributions from the Research Council of Norway (196438/BIOWAVE and 207541/OILWAVE) for analyzing field data. The authors would like to thank Svein Sundby and Frode Vikebø (IMR) for helpful discussions and kind assistance during the planning phase, and Erik Berg (IMR), as well as the captain and crew of R/V *Johan Hjort*, for their kind assistance with the drifter deployments. We would also like to thank Ronald Pedersen (IMR), Tor Gammelsrød (UiB), Erik Kvaleberg and Anne Hesby (Royal Navy) for loan of instruments and assistance with the ADCP rig. Assistance from the captains and crews of the NSO Crusader and R/V *Håkon Mosby* when deploying and recovering the ADCP rig is also gratefully acknowledged.

References

Albretsen, J., Sperrevik, A. K., Staalstrøm, A., Sandvik, A. D., Vikebø, F., and Asplin, L.: NorKyst-800 report no. 1: User manual and technical descriptions, Tech. Rep. 2, Institute of Marine Researh, Bergen, Norway, available at: http://www.imr.no/filarkiv/2011/07/fh_2-2011_til_web.pdf/nb-no (last access: 2 June 2014), 2011. 1366

Barrick, D. E., Evans, M. W., and Weber, B. L.: Ocean Surface Currents Mapped by Radar, Science, 198, 138–144, 1977. 1359

Barth, A., Alvera-Azcárate, A., and Weisberg, R. H.: Assimilation of high-frequency radar currents in a nested model of the West Florida Shelf, J. Geophys. Res.-Oceans, 113, C08033, doi:10.1029/2007JC004585, 2008. 1359

Blockley, E. W., Martin, M. J., McLaren, A. J., Ryan, A. G., Waters, J., Lea, D. J., Mirouze, I., Peterson, K. A., Sellar, A., and Storkey, D.: Recent development of the Met Office operational ocean forecasting system: an overview and assessment of the new Global FOAM forecasts, Geosci. Model Dev. Discuss., 6, 6219–6278, doi:10.5194/gmdd-6-6219-2013, 2013. 1359

Brassington, G. B., Pugh, T., Spillman, C., Schulz, E., Beggs, H., Schiller, A., and Oke, P. R.: BLUElink Development of operational oceanography and servicing, Journal of Research and Practice in Information Technology, 39, 151–164, 2007. 1359

OSD

11, 1357–1390, 2014

Breivik, Ø. and Sætra, Ø.: Real time assimilation of HF radar currents into a coastal ocean model, J. Marine Syst., 28, 161–182, 2001. 1359

Chapman, D. C.: Numerical treatment of cross-shelf open boundaries in a barotropic coastal ocean model, J. Phys. Oceanogr., 15, 1060–1075, 1985. 1367

Chapman, R., Shay, L., Graber, H., Edson, J., Karachintsev, A., Trump, C., and Ross, D.: On the accuracy of HF radar surface current measurements: intercomparisons with ship-based sensors, J. Geophys. Res.-Oceans (1978–2012), 102, 18737–18748, 1997. 1359, 1360, 1365

Courtier, P., Thépaut, J.-N., and Hollingsworth, A.: A strategy for operational implementation of 4D-Var, using an incremental approach, Q. J. Roy. Meteor. Soc., 120, 1367–1387, 1994. 1359

Davis, R. E.: Drifter observations of coastal surface currents during CODE: The method and descriptive view, J. Geophys. Res.-Oceans, 90, 4741–4755, 1985. 1369

Dimet, F.-X. L. E., and Talagrand, O.: Variational algorithms for analysis and assimilation of meteorological observations: theoretical aspects, Tellus A, 38, 97–110, 1986. 1359

Evensen, G.: The Ensemble Kalman Filter: theoretical formulation and practical implementation, Ocean Dynam., 53, 343–367, 2003. 1359

Flather, R. A.: A tidal model of the north-west European continental shelf, Memoires de la Society Royal des Sciences de Liege, 10, 141–164, 1976. 1367

Fu, L.-L., Christensen, E. J., Yamarone, C. A., Lefebvre, M., Ménard, Y., Dorrer, M., and Escudier, P.: TOPEX/POSEIDON mission overview, J. Geophys. Res.-Oceans, 99, 24369–24381, 1994. 1358

Gurgel, K.-W., Antonischki, G., Essen, H.-H., and Schlick, T.: Wellen Radar (WERA): a new ground-wave HF radar for ocean remote sensing, Coast. Eng., 37, 219–234, 1999. 1359

Isachsen, P.: Baroclinic instability and eddy tracer transport across sloping bottom topography: How well does a modified Eady model do in primitive equation simulations?, Ocean Model., 39, 183–199, 2011. 1362

Kjelaas, A. G. and Whelan, C.: Rapidly deployable SeaSonde for modeling oil spill response, Sea Technol., 52, 10–13, 2011. 1359

Kristiansen, J., Bjørge, D., Berge, H., Simonsen, M., Torheim, T., Aasen, I.-L., Rooney, G., and Edwards, J.: Improving the screen temperature forecasts of the Norwegian configuration of the UM: on model interoperability with respect to soil initial conditions, in: Unified Model User Workshop, Exeter, UK, 9–11 November 2009, 2009. 1367

OSD
11, 1357–1390, 2014

Liu, Y. and Weisberg, R. H.: Evaluation of trajectory modeling in different dynamic regions using normalized cumulative Lagrangian separation, J. Geophys. Res.-Oceans, 116, C09013, doi:10.1029/2010JC006837, 2011. 1370

Marchesiello, P., McWilliams, J. C., and Shchepetkin, A.: Open boundary conditions for long-term integration of regional oceanic models, Ocean Model., 3, 1–20, 2001. 1367

Moore, A. M., Arango, H. G., Di Lorenzo, E., Miller, A. J., and Cornuelle, B. D.: An adjoint sensitivity analysis of the southern California current circulation and ecosystem, J. Phys. Oceanogr., 39, 702–720, 2009. 1363

Moore, A. M., Arango, H. G., Broquet, G., Edwards, C., Veneziani, M., Powell, B., Foley, D., Doyle, J. D., Costa, D., and Robinson, P.: The Regional Ocean Modeling System (ROMS) 4-dimensional variational data assimilation systems: Part II – Performance and application to the California current system, Prog. Oceanogr., 91, 50–73, 2011a. 1359

Moore, A. M., Arango, H. G., Broquet, G., Edwards, C., Veneziani, M., Powell, B., Foley, D., Doyle, J. D., Costa, D., and Robinson, P.: The Regional Ocean Modeling System (ROMS) 4-dimensional variational data assimilation systems: Part {III} – Observation impact and observation sensitivity in the California Current System, Prog. Oceanogr., 91, 74–94, 2011b. 1359

Moore, A. M., Arango, H. G., Broquet, G., Powell, B. S., Weaver, A. T., and Zavala-Garay, J.: The Regional Ocean Modeling System (ROMS) 4-dimensional variational data assimilation systems: Part I – System overview and formulation, Prog. Oceanogr., 91, 34–49, 2011c. 1359, 1366

Oke, P. R., Allen, J. S., Miller, R. N., Egbert, G. D., and Kosro, P. M.: Assimilation of surface velocity data into a primitive equation coastal ocean model, J. Geophys. Res.-Oceans, 107, 3122, doi:10.1029/2000JC000511, 2002. 1359

Oke, P. R., Brassington, G. B., Griffin, D. A., and Schiller, A: Ocean data assimilation: a case for ensemble optimal interpolation, Australian Meteorological and Oceanographic Journal, 59, 67–76, 2010. 1359

Paduan, J. D. and Shulman, I.: HF radar data assimilation in the Monterey Bay area, J. Geophys. Res.-Oceans, 109, C07S09, doi:10.1029/2003JC001949, 2004. 1359

Rayner, N., Parker, D., Horton, E., Folland, C., Alexander, L., Rowell, D., Kent, E., and Kaplan, A.: Global analyses of sea surface temperature, sea ice, and night marine air temperature since the late nineteenth century, J. Geophys. Res.-Atmos., 108, 4407, doi:10.1029/2002JD002670, 2003. 1358

OSD
11, 1357–1390, 2014

Roemmich, D., Johnson, G. C., Riser, S., Davis, R., Gilson, J., Owens, W. B., Garzoli, S. L., Schmid, C., and Ignaszewski, M.: The Argo Program: Observing the Global Ocean with Profiling Floats, 2009. 1358

Röhrs, J., Christensen, K., Hole, L., Broström, G., Drivdal, M., and Sundby, S.: Observation-based evaluation of surface wave effects on currents and trajectory forecasts, Ocean Dynam., 62, 1519–1533, 2012. 1361, 1369

Röhrs, J., Christensen, H. K., Vikebø, B., F., Sundby, S., Saetra, O., and Broström, G.: Wave-induced transport and vertical mixing of pelagic eggs and larvae, Limnol. Oceanogr., in press, 2014. 1366

Sakov, P., Counillon, F., Bertino, L., Lisæter, K. A., Oke, P. R., and Korablev, A.: TOPAZ4: an ocean-sea ice data assimilation system for the North Atlantic and Arctic, Ocean Sci., 8, 633–656, doi:10.5194/os-8-633-2012, 2012. 1359

Wentz, F. J., Gentemann, C., Smith, D., and Chelton, D.: Satellite measurements of sea surface temperature through clouds, Science, 288, 847–850, 2000. 1358

Zhang, W. G., Wilkin, J. L., Levin, J. C., and Arango, H. G.: An adjoint sensitivity study of buoyancy- and wind-driven circulation on the New Jersey inner shelf, J. Phys. Oceanogr., 39, 1652–1668, 2009. 1363

Zhang, W. G., Wilkin, J. L., and Arango, H. G.: Towards an integrated observation and modeling system in the New York bight using variational methods, Part I: 4DVAR data assimilation, Ocean Model., 35, 119–133, 2010. 1359, 1360

OSD
11, 1357–1390, 2014

Table 1. Standard deviation of analysis error in idealized experiments: comparison between different error correlation scales.

	STD(u) [m s^{-1}]	STD(v) [m s^{-1}]	STD(T) [K]
NONE	0.183	0.223	0.511
5 km	0.168	0.209	0.437
10 km	0.174	0.216	0.447
20 km	0.180	0.223	0.452

OSD
11, 1357–1390, 2014

Table 2. Standard deviation of analysis error in idealized experiments: comparison between different observation data sets.

	STD(u) [m s^{-1}]	STD(v) [m s^{-1}]	STD(T) [K]
NONE	0.183	0.223	0.511
HF	0.150	0.188	0.442
CTD	0.183	0.223	0.471
ALL	0.168	0.209	0.437

OSD
11, 1357–1390, 2014

Table 3. Skill score during analysis and forecast when comparing with the two different surface drifter types.

Observation set	Analysis		Forecast	
	iSLDMB	iSPHERE	iSLDMB	iSPHERE
CTRL	0.42	0.16	0.18	0.21
HF	0.44	0.21	0.30	0.26
CTD	0.40	0.15	0.16	0.19
ALL	0.43	0.21	0.33	0.22

OSD
11, 1357–1390, 2014

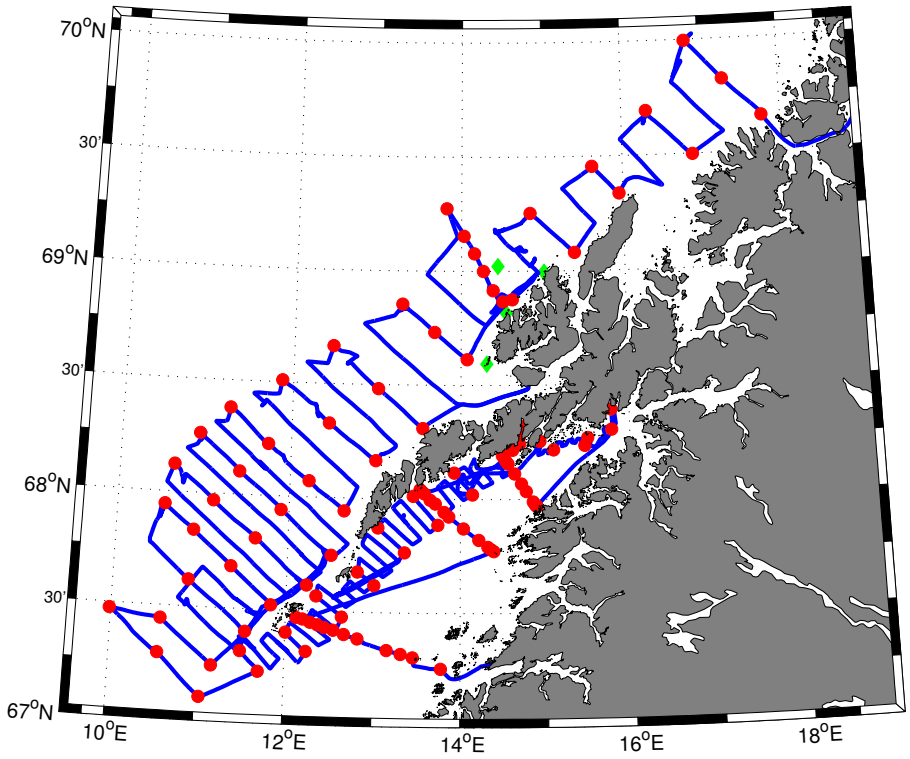

Figure 1. The ship track of R/V *Johan Hjort* during the cod stock assessment cruise in March 2013. The cruise started in Tromsø (north east in map) and ended in Bodø (bottom middle of map). The red dots indicate stations where CTD profiles where taken. The positions of the three HF radars and the ADCP rig are shown as green diamonds.

OSD
11, 1357–1390, 2014

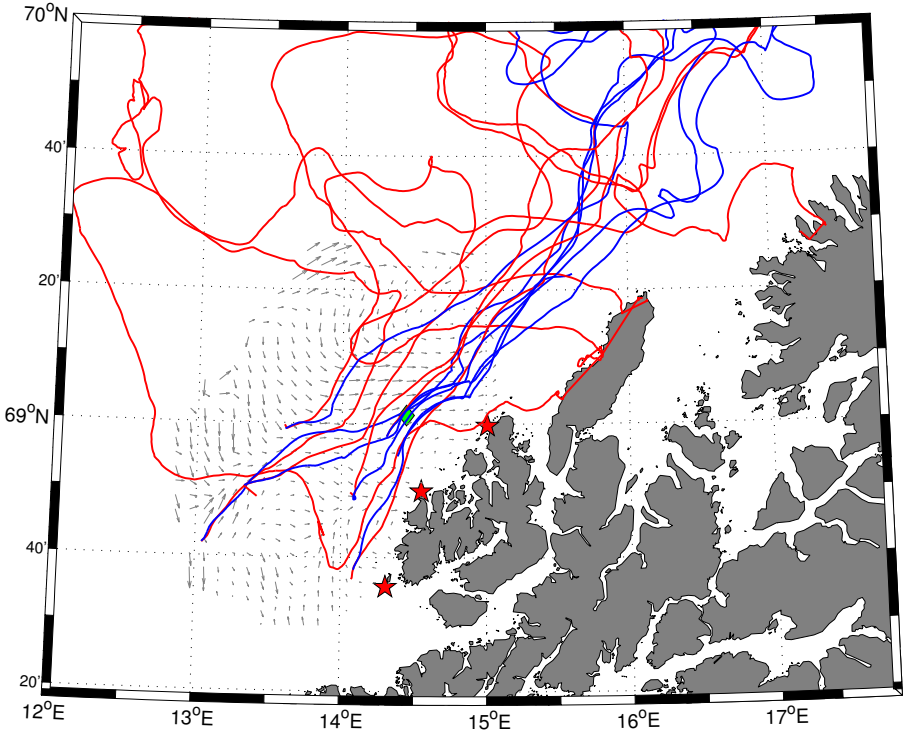

Figure 2. Positions of the HF radar stations, drifter trajectories, and ADCP rig. Starting from the south the HF radar stations are LITLØY, HOVDEN, and NYKSUND. The grey arrows are total vector currents from the HF radar system, indicative of the coverage when all three stations were operational. The iSphere trajectories are red, while the iSLDMB trajectories are blue. The position of the ADCP rig is marked by a green diamond.

OSD
11, 1357–1390, 2014

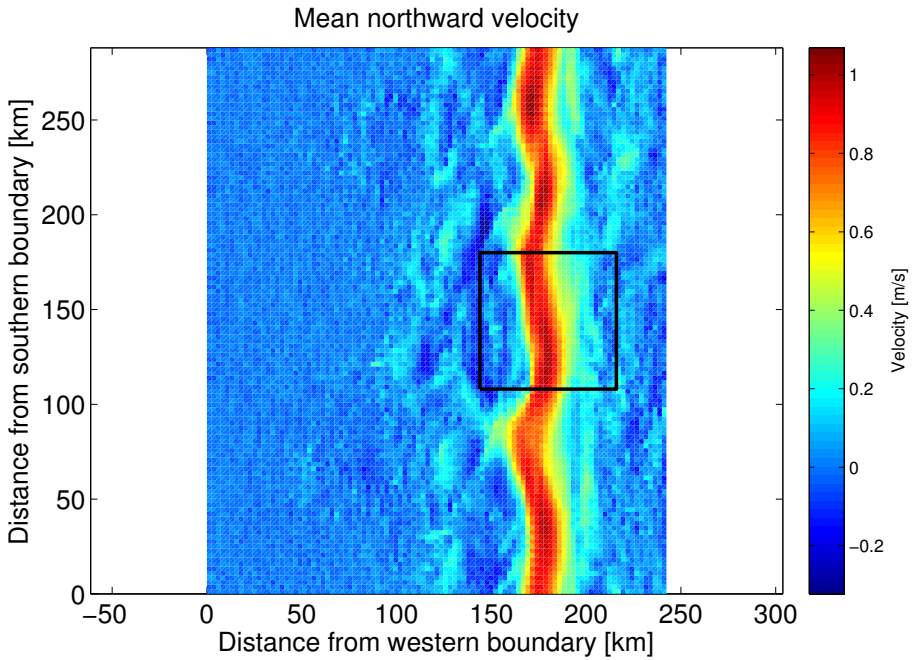

Figure 3. The mean northward surface velocity during a three days simulation. The region enclosed by the black line is used for assessing the performance of the data assimilation system.

OSD
11, 1357–1390, 2014

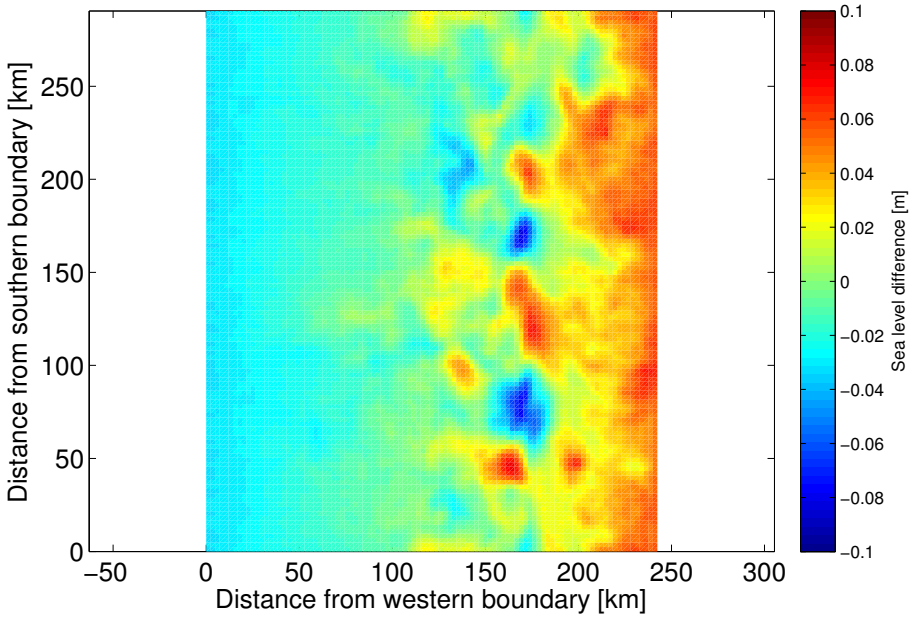

Figure 4. The difference between the restart fields used for the assimilation experiments and for obtaining synthetic observations, here showing sea surface height.

OSD
11, 1357–1390, 2014

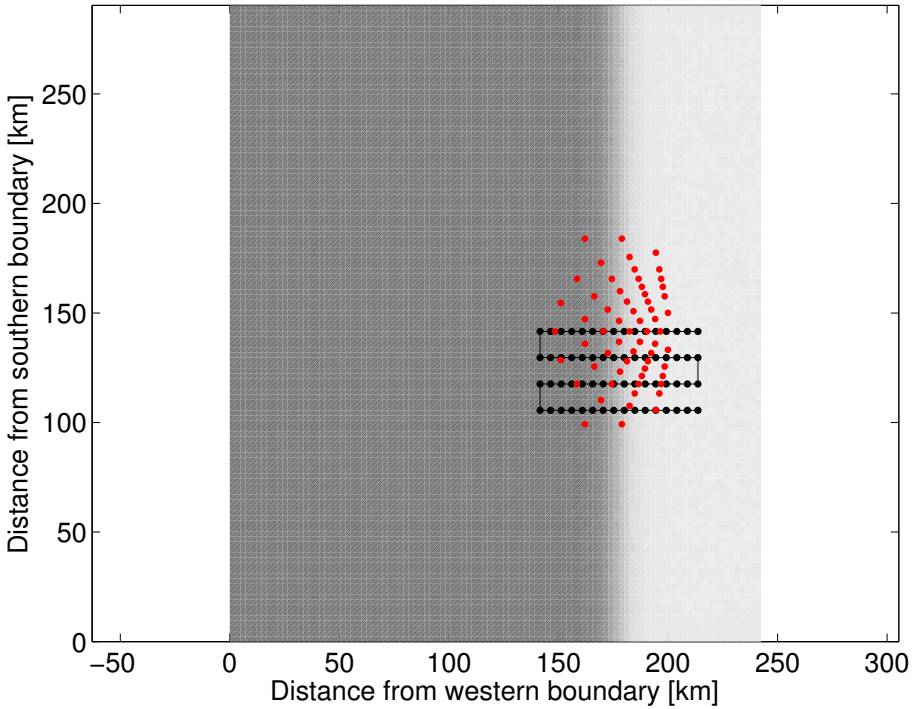

Figure 5. The black dots show where temperature profiles are taken. One full vertical profile is taken every hour, and four sections are made, starting from the north. The red dots are the intersection points of the two simulated HF radars. Hourly observations of total current vectors are produced for the assimilation. The water depth is indicated in gray and ranges from 200 m on the shelf (light gray) and 1800 m in the deep part (dark gray).

OSD
11, 1357–1390, 2014

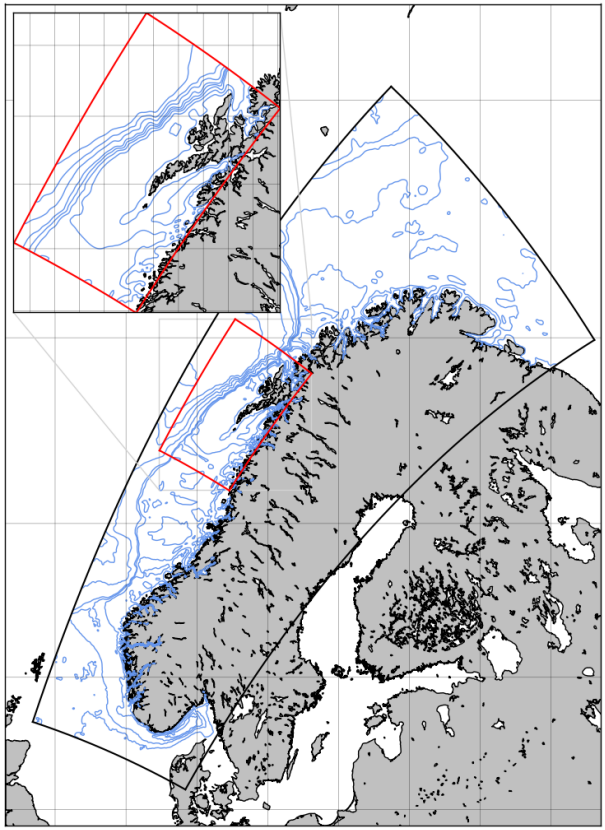

Figure 6. The model domain. The full domain of "NorKyst800" is shown with black border, while our coarser subdomain is shown with red border.

OSD
11, 1357–1390, 2014

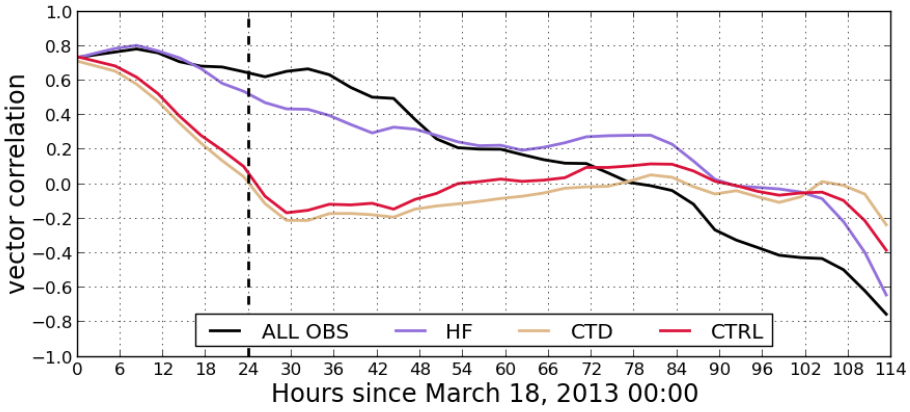

Figure 7. Vector correlation as a function of time. The vertical line indicates the shift from the analysis to the forecast period. A value of 1 means perfect correlation in both speed and direction, a value of 0 means no correlation, while a value of −1 means that the velocities are anticorrelated, i.e. same speeds but opposite directions

OSD
11, 1357–1390, 2014

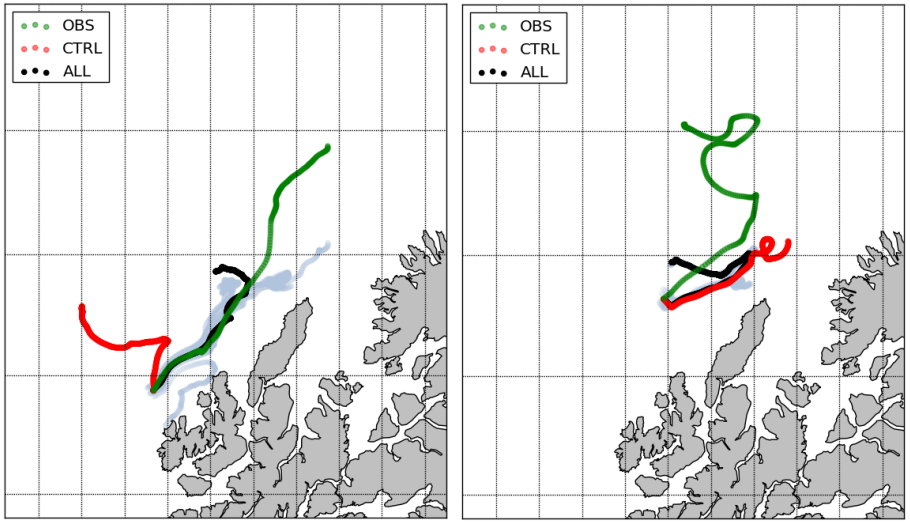

Figure 8. The figure show drifter pathways for two different drifters as observed (green), predicted by CTRL (red) and predicted by ALL (black). Additionaly, the grey tracks shows the pathways of the perturbed initial position floats. The trajectories shown here were released at the start of the analysis

OSD
11, 1357–1390, 2014

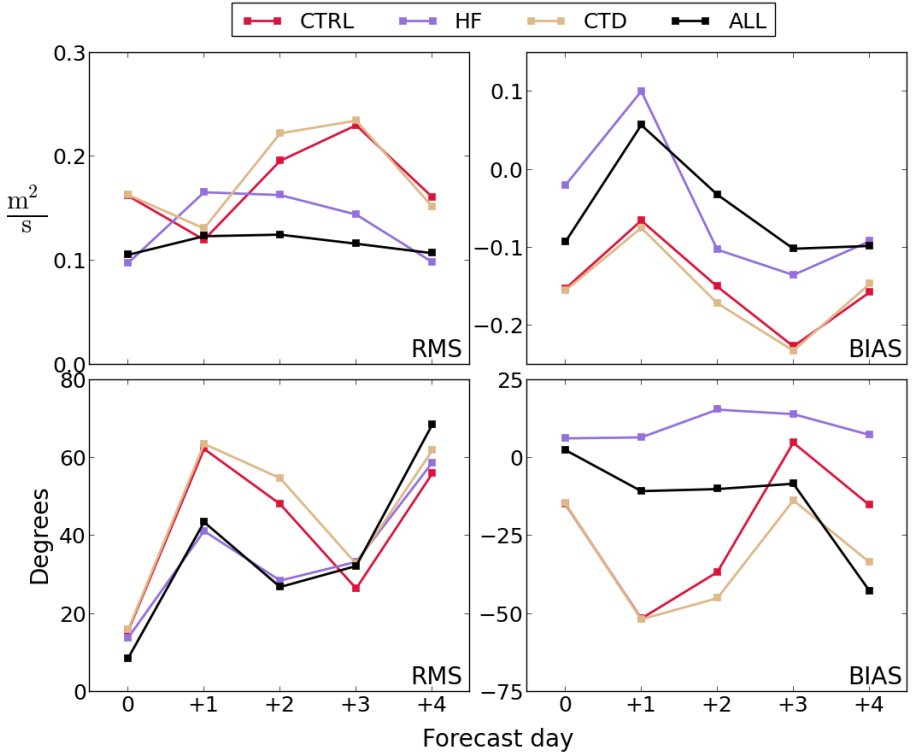

Figure 9. RMS and BIAS of transport speed (upper panels) and direction (lower panels) in the water column stretching from 0.5–8 m below the surface, as a function of forecast day.

OSD
11, 1357–1390, 2014

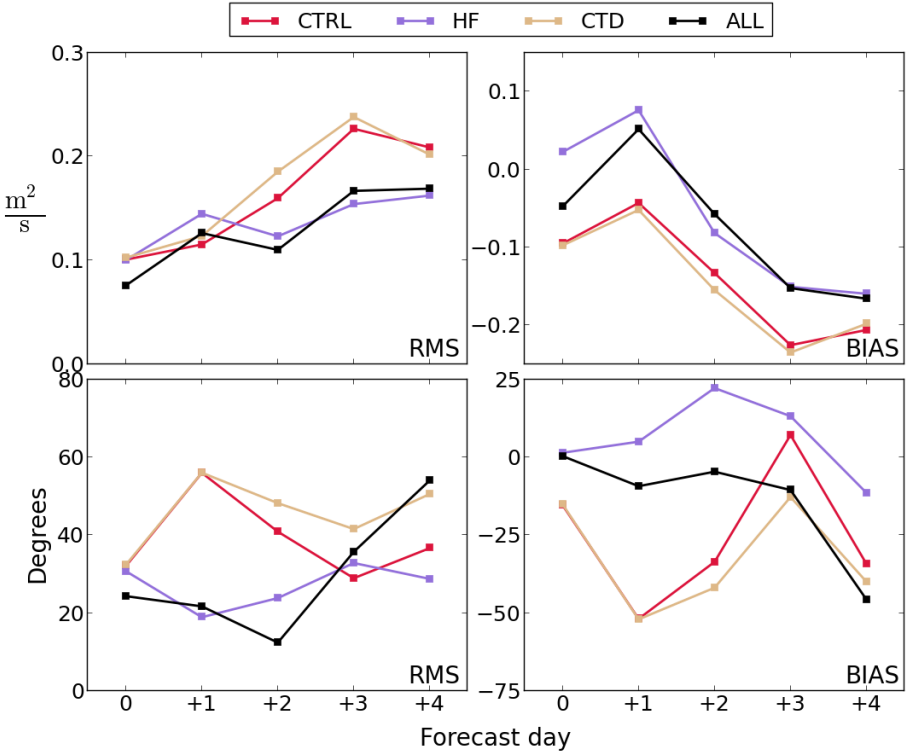

Figure 10. RMS and BIAS of transport speed (upper panels) and direction (lower panels) in the water column stretching from 8–41 m below the surface, as a function of forecast day.

OSD
11, 1357–1390, 2014